A Killer-Protector System Regulates Both Hybrid Sterility and Segregation Distortion in Rice

Jiangyi Yang *et al.*

Science **337**, 1336 (2012);
DOI: 10.1126/science.1223702

Science (print ISSN 0036-8075; online ISSN 1095-9203) is published weekly, except the last week in December, by the American Association for the Advancement of Science, 1200 New York Avenue NW, Washington, DC 20005.

proteins were coexpressed (fig. S17B). However, microtubules did not eliminate ROP11 or MIDD1$^{\Delta N}$ when ROP11 or MIDD1$^{\Delta N}$ was solely expressed (fig. S17, A and C). In contrast, cortical microtubules eliminated MIDD$^{\Delta N}$-AD, in which a minimal plasma membrane–anchor domain from ROP11 (*19*) was fused to MIDD$^{\Delta N}$ (fig. S17D). These results suggest that MIDD1 mediates elimination of ROP11 from the plasma membrane by the cortical microtubules, probably by the mechanism in which plasma membrane–associated cortical microtubules physically interfere the plasma membrane–anchored MIDD1-ROP11 complexes.

We show that secondary wall pattern is established by two processes: a ROP-driven symmetry breaking and a mutual inhibitory interaction between cortical microtubules and active ROP domains (fig. S18). The first process may be explained by Turing's reaction diffusion model (*20*), where ROPGEF4 and ROPGAP3 act as an activator and an inhibitor, respectively. This model requires a positive feedback of the activator. In yeast, a scaffold protein, Bem1p, mediates a positive feedback of Cdc24p GEF (*21*). A similar scaffold protein might function with ROPGEF4. In the second process, MIDD1 promotes disassembly at the microtubule tip (*5*), whereas MIDD1 mediates the elimination of active ROPs at the microtubule sides. MIDD1 may interact with AtKinesin-13A (*8*) as well as ROP11 and cortical microtubules. MIDD1 may have different functions at the tip and side of cortical microtubules.

We showed that MIDD1-mediated interaction between spontaneously activated ROP domains and cortical microtubules produces pitted pattern of metaxylem cells. Although *ropgef4* did not affect significantly protoxylem cell wall patterns, because not only MIDD1 but also members of ROPs are also expressed in protoxylem cells (*22*), such secondary wall patterns as annular, spiral, and reticulate patterns might be produced by similar MIDD1-mediated interaction between activated ROP domains and cortical microtubules. Indeed, stabilization of microtubules with taxol produced a reticulate-like secondary wall pattern in developing metaxylem cells. Differences among ROPGEF and/or ROPGAP members may also contribute to size differences of activated ROP domains and then of the secondary wall depleted area. Our reconstitution assay may be a powerful tool to test this idea.

MIDD1 is expressed in not only xylem cells but also nonxylem cells (*23*). Considering the nature of MIDD1, even in nonxylem cells, MIDD1 may function in production of specific patterns of cortical microtubules and of activated ROP domains. As shown in epidermal pavement cells, local ROP domain activation and microtubule organization underlie local polarized growth of the cell (*1*). Thus, MIDD1-mediated membrane domain establishment may contribute to the formation of various plant cell shapes generally.

References and Notes

1. Z. Yang, *Annu. Rev. Cell Dev. Biol.* **24**, 551 (2008).
2. J. Dong, D. C. Bergmann, *Curr. Top. Dev. Biol.* **91**, 267 (2010).
3. J. Dettmer, J. Friml, *Curr. Opin. Cell Biol.* **23**, 686 (2011).
4. C. G. Rasmussen, J. A. Humphries, L. G. Smith, *Annu. Rev. Plant Biol.* **62**, 387 (2011).
5. Y. Oda, Y. Iida, Y. Kondo, H. Fukuda, *Curr. Biol.* **20**, 1197 (2010).
6. M. Lavy *et al.*, *Curr. Biol.* **17**, 947 (2007).
7. S. Li, Y. Gu, A. Yan, E. Lord, Z. B. Yang, *Mol. Plant* **1**, 1021 (2008).
8. E. Mucha, C. Hoefle, R. A. Hückelhoven, A. Berken, *Eur. J. Cell Biol.* **89**, 906 (2010).
9. S. J. Heasman, A. J. Ridley, *Nat. Rev. Mol. Cell Biol.* **9**, 690 (2008).
10. P. Perez, S. A. Rincón, *Biochem. J.* **426**, 243 (2010).
11. K. Ohashi-Ito, Y. Oda, H. Fukuda, *Plant Cell* **22**, 3461 (2010).
12. J. Zuo, Q. W. Niu, N. H. Chua, *Plant J.* **24**, 265 (2000).
13. Z. L. Zheng, Z. Yang, *Plant Mol. Biol.* **44**, 1 (2000).
14. A. Berken, C. Thomas, A. Wittinghofer, *Nature* **436**, 1176 (2005).
15. Y. Gu, S. Li, E. M. Lord, Z. Yang, *Plant Cell* **18**, 366 (2006).
16. G. Wu, H. Li, Z. Yang, *Plant Physiol.* **124**, 1625 (2000).
17. Y. Zhang, S. McCormick, *Proc. Natl. Acad. Sci. U.S.A.* **104**, 18830 (2007).
18. C. A. Moores, R. A. Milligan, *J. Cell Sci.* **119**, 3905 (2006).
19. M. Lavy, S. Yalovsky, *Plant J.* **46**, 934 (2006).
20. A. M. Turing, *Proc. R. Soc. London Ser. B* **237**, 37 (1952).
21. L. Kozubowski *et al.*, *Curr. Biol.* **18**, 1719 (2008).
22. M. Yamaguchi *et al.*, *Plant J.* **66**, 579 (2011).
23. D. Winter *et al.*, *PLoS One* **2**, e718 (2007).

Acknowledgments: We thank N. Chua of the Rockefeller University for providing the pER8 vector; U. Grossniklaus of the University of Zurich for providing the pMDC7 vector; T. Nakagawa of Shimane University for providing the pGWB vectors; Y. Ohya of the University of Tokyo for critical reading of this manuscript; A. Nakano, T. Ueda, and S. Betsuyaku of the University of Tokyo for technical advice; and Y. Nakashima for technical assistance. This work was supported partly by Grants-in-Aid from the Ministry of Education, Science, Sports and Culture of Japan (19060009) to H.F.; from the Japan Society for the Promotion of Science to H.F. (23227001) and Y.O. (22870005) and the NC-CARP project; and from JST, Precursory Research for Embryonic Science and Technology (PRESTO) to Y.O. (20103).

Supplementary Materials

www.sciencemag.org/cgi/content/full/337/6100/1333/DC1
Materials and Methods
Figs. S1 to S18
Table S1
References (*24*, *25*)

29 March 2012; accepted 9 July 2012
10.1126/science.1222597

A Killer-Protector System Regulates Both Hybrid Sterility and Segregation Distortion in Rice

Jiangyi Yang,[1]* Xiaobo Zhao,[1]* Ke Cheng,[1]* Hongyi Du,[1] Yidan Ouyang,[1] Jiongjiong Chen,[1] Shuqing Qiu,[1] Jianyan Huang,[1] Yunhe Jiang,[1] Liwen Jiang,[2] Jihua Ding,[1] Jia Wang,[1] Caiguo Xu,[1] Xianghua Li,[1] Qifa Zhang[1]†

Hybrid sterility is a major form of postzygotic reproductive isolation that restricts gene flow between populations. Cultivated rice (*Oryza sativa* L.) consists of two subspecies, *indica* and *japonica*; inter-subspecific hybrids are usually sterile. We show that a killer-protector system at the *S5* locus encoded by three tightly linked genes [*Open Reading Frame 3 (ORF3)* to *ORF5*] regulates fertility in *indica-japonica* hybrids. During female sporogenesis, the action of ORF5+ (killer) and ORF4+ (partner) causes endoplasmic reticulum (ER) stress. ORF3+ (protector) prevents ER stress and produces normal gametes, but ORF3− cannot prevent ER stress, resulting in premature programmed cell death and leads to embryo-sac abortion. Preferential transmission of *ORF3*+ gametes results in segregation distortion in the progeny. These results add to our understanding of differences between *indica* and *japonica* rice and may aid in rice genetic improvement.

Reproductive isolation is both an indicator of speciation and a mechanism for maintaining species identity. The Dobzhansky-Muller model (*1*) suggests that hybrid incompatibility results from deleterious interactions between independently evolved loci from diverged populations. Studies in animal models such as *Drosophila* and mice have identified several of such interactive genes that cause hybrid incompatibility and segregation distortion (*2*, *3*). In plants, hybrid sterility is a major form of postzygotic reproductive isolation, and several genes have been identified that conform to the Dobzhansky-Muller model for reproductive isolation (*4*–*7*). Hybrid sterility between *indica* and *japonica* subspecies of cultivated rice (*Oryza sativa* L.) is one example of postzygotic reproductive isolation in plants (*8*–*10*). Genetic analyses of *indica-japonica* hybrids have identified a large number of loci conditioning hybrid sterility (*10*). Several genes for *indica-japonica* hybrid sterility (*11*–*13*) and interspecific hybrid sterility between *O. sativa* and *O. glumaepatula* (*14*) were recently cloned, aiding in our understanding of the biological processes of hybrid sterility in rice species.

[1]National Key Laboratory of Crop Genetic Improvement and National Centre of Plant Gene Research, Huazhong Agricultural University, Wuhan 430070, China. [2]School of Life Sciences, Chinese University of Hong Kong, Shatin, New Territories, Hong Kong 999077, China.

*These authors contributed equally to this work.
†To whom correspondence should be addressed. E-mail: qifazh@mail.hzau.edu.cn

S5 is a major locus for hybrid sterility in rice that affects embryo-sac fertility, as identified in a number of studies across a range of germplasms (*11*, *15*–*19*). The *S5* locus has three alleles, an *indica* allele *S5*-i, a *japonica* allele *S5*-j, and a neutral allele *S5*-n (*15*). Hybrids of genotype *S5*-i/*S5*-j are mostly sterile, whereas hybrids of genotypes consisting of *S5*-n with either *S5*-i or *S5*-j are mostly fertile (*15*–*17*). The *S5* region has been mapped (*18*) and covers up to five open reading frames (*ORF1* to *ORF5*). Transformation studies of *ORF3* to *ORF5* (*11*) from an *indica* variety into a *japonica* variety showed reduced fertility, due to embryo-sac abortion, for transformants harboring *indica ORF5*, whereas the fertility of transformants of *ORF3* and *ORF4* was not affected. The *indica* and *japonica* alleles of *ORF5*, which encodes an aspartic protease, differ by two nucleotides, whereas the wide compatibility allele has a large deletion in the N terminus of the predicted protein, causing subcellular mislocalization of the protein (*11*).

Because segregation distortion has been observed in progenies of *indica-japonica* hybrids (*12*, *19*, *20*), we assayed *S5* genotypes of 195 seedlings from a BC_6F_1 plant BL(BL/NJ), a near isogenic line (NIL) heterozygous for the *S5*-i allele from an *indica* variety Nanjing 11, backcrossing successively with a *japonica*-variety Balilla. The resulting progeny showed genotypes deviating from the expected 1:2:1 ratio (Table 1). A maximum likelihood estimate for the frequency of *S5*-j transmitted via the female gametes was 0.1, compared with the expected 0.5. Similar segregation distortion was also observed in progenies from other *indica-japonica* crosses (Table 1).

Because it is difficult to explain the hybrid sterility and segregation distortion by *ORF5* alone, we determined genomic sequences of *ORF1* to *ORF4* for Nanjing 11 (*indica*), Balilla (*japonica*), Dular, and 02428 (the latter two are wide compatibility varieties that can produce highly fertile hybrids in crosses with either *indica* or *japonica*). Sequence polymorphisms with predictable functional changes among the genotypes in the predicted proteins were observed in ORF3 and ORF4 but not ORF1 or ORF2 (fig. S1). By investigating the transcripts, we observed that the translation start codons of *ORF4* and *ORF5* were located only 0.8 kb away, but the genes were transcribed in opposite directions. The *ORF4* sequence of Balilla and 02428 was predicted to encode a protein with a transmembrane domain and had no homology with any known proteins (fig. S2). An 11–base pair (bp) deletion predicted to cause premature termination of the predicted protein and a loss of the putative transmembrane domain (fig. S2) was detected in ORF4 of Nanjing 11 and Dular relative to Balilla and 02428 (fig. S1). *ORF3* was mapped 11.7 kb away from *ORF4* and showed homology to a heat shock protein Hsp70 gene. The *ORF3* sequences of Balilla and Dular have a 13-bp deletion relative to the other two genotypes (fig. S1), which results in a frameshift in the C terminus of the protein (fig. S3). On the basis of the sequence differences in these ORFs (fig. S1), we designated the *ORF3* allele from Nanjing 11 and 02428 as *ORF3*+ and the other allele as *ORF3*–; the *ORF4* allele from Balilla and 02428 as *ORF4*+ and the other one as *ORF4*–; and the *ORF5* allele from Nanjing 11 as *ORF5*+, the one from Balilla as *ORF5*–, and those from Dular and 02428 as *ORF5n*.

We tested the effect of *ORF3* on hybrid sterility by crossing a transgenic Balilla*ORF3*+ plant [in which *ORF3*+ from Nanjing 11 was transformed into Balilla and showing normal fertility (Table 2)] with BL(NJ/NJ), a NIL in which the *S5* fragment contains *ORF3* to *ORF5* from Nanjing 11 (*ORF3*+, *ORF4*–, and *ORF5*+) introgressed into a Balilla background (*ORF3*–, *ORF4*+, and *ORF5*–). A Balilla and BL(NJ/NJ) cross typically produces hybrid with reduced fertility (Table 1). However, BL/NJ*ORF3*+ plants from this cross showed 71.5% spikelet fertility, compared with 50.3% of the BL/NJ plants (Table 2). This rescue was confirmed in the progeny of heterozygous plants BL/NJ*ORF3*+, in which the fertility of BL/NJ*ORF3*+ plants (75.1%) was much higher than that of BL/NJ plants (46.8%). Therefore, we inferred that *ORF3*+ rescued fertility of the *indica-japonica* hybrid, presumably by protecting the gametes from the killing effect of *ORF5*+. Comparison between normal and *ORF3*+-rescued plants [BL/BL or NJ/NJ versus BL/NJ*ORF3* (Table 2)] showed that the fertility-protecting effect of *ORF3*+ is only partial. We suspect that the independent transmission of the transformed hemizygous *ORF3*+ relative to the host *S5* locus explains these observations because we would expect only approximately half of the gametes to inherit the *ORF3*+ transgene, which would be protected from killing by *ORF5*+.

To support our hypothesis, we crossed Balilla*ORF3*+ carrying a transformed *ORF3*+

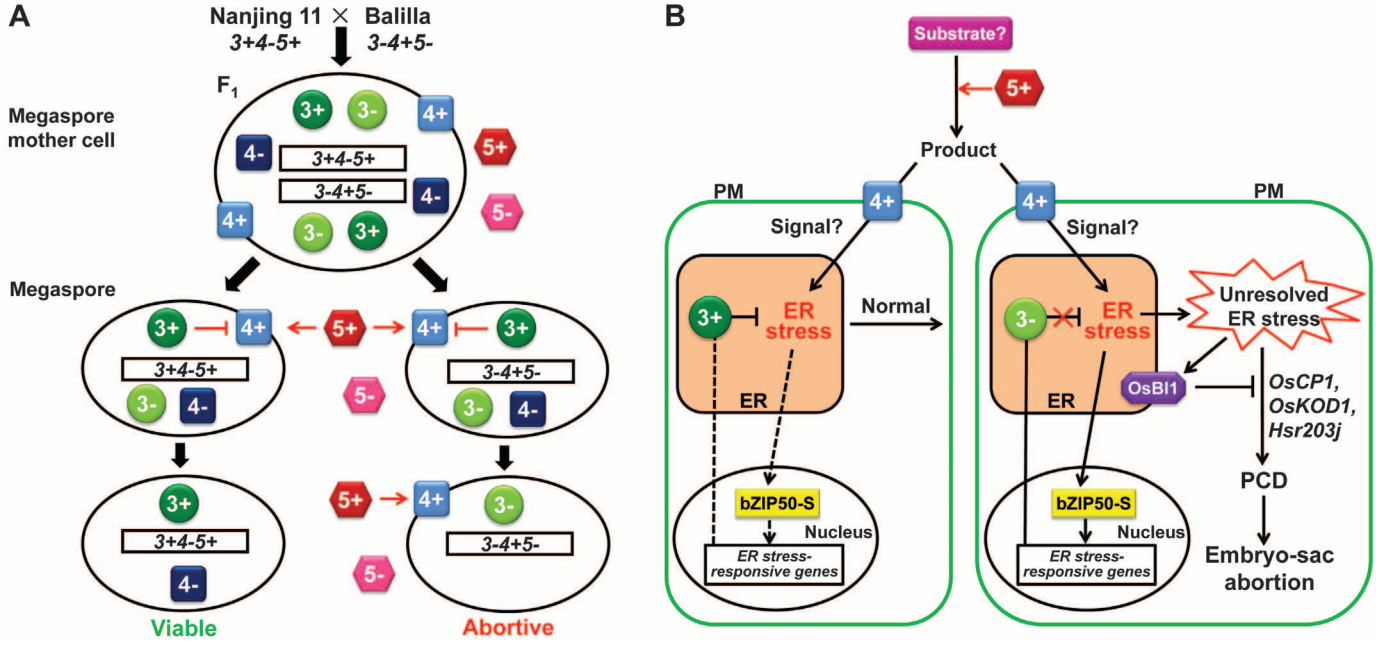

Fig. 1. Schematic representation of the killer-protector system in an *indica-japonica* hybrid regulated by the *S5* locus. (**A**) A genetic model depicting the process of megaspore formation and effects of the three genes, where 3+, 3–, 4+, 4–, 5+, and 5– represent ORF3+, ORF3–, ORF4+, ORF4–, ORF5+, and ORF5–, respectively, and colored blocks and circles represent the proteins. In the megaspore mother cell and daughter cells immediately after meiotic division, killing would not occur because of the presence of ORF3+. Killing would occur in the daughter cell carrying ORF3– and ORF4+ at a later stage of megaspore development. (**B**) Hypothetical molecular processes involving ER-stress and PCD. bZIP50-S, spliced bZIP50; ER, endoplasmic reticulum; PM, plasma membrane.

and Balilla*ORF5*+ carrying a transformed *ORF5*+ (Table 2). The progeny plants lacking any transgene were fully fertile, as expected, as were the ones carrying *ORF3*+ alone. Transgenic *ORF5*+ plants were sterile, whereas the addition of transgene *ORF3*+ rescued the fertility of the plants.

Transforming *ORF4*+ into BL(NJ/NJ) resulted in no fertility reduction in BL(NJ/NJ)*ORF4*+ transformants (Table 3), as expected, because of the presence of the protector *ORF3*+ in the introgressed fragment. Also, the fertility of hybrids involving the Dular fragment (*ORF3*–, *ORF4*–, and *ORF5n*) from the BL(BL/DL) × BL(BL/NJ) cross was normal, regardless of whether the allelic fragment was *indica* or *japonica* (Table 3). However, in the F_1 progeny from a BL(NJ/NJ)*ORF4*+ × BL(DL/DL) cross, individuals with the transgene BL(DL/NJ)*ORF4*+ exhibited reduced spikelet fertility (39.3%), compared with the transgene-negative plants BL(DL/NJ) or the parental BL(NJ/NJ)*ORF4*+. Furthermore, statistically significant segregation distortion at the *S5* locus was observed in the F_2 progeny produced from BL(DL/NJ)*ORF4*+ plants (Table 3), in which the NJ fragment (estimated frequency 0.654) was favored at the cost of the DL fragment (0.346). Consequently, the frequency of DL/DL homozygote was deficient compared with the expected 1:2:1 ratio. Thus, the addition of *ORF4*+ in this hybrid resulted in the death of gametes with the Dular fragment.

To examine the role of *ORF4*+ in relation to *ORF5*+, we crossed BL(BL/DL) with Balilla*ORF5*+ (Table 3). Among F_1, the two genotypes with the transformed *ORF5*+ (BL/BL*ORF5*+ and BL/DL*ORF5*+) were mostly sterile, whereas their transgene-negative counterparts were fertile. This was also observed in the F_2 segregants of this cross. Moreover, DL/DL*ORF5*+, which is homozygous for the Dular genotype with an added *ORF5*+, showed normal fertility, and fertility of BL(BL/NJ) was not affected by the transformed *ORF5*+. Given that both Balilla and Dular had *ORF3*– and nonkiller ORF5, the fertility difference between BL/DL*ORF5*+ and DL/DL*ORF5*+ can be ascribed to differences in ORF4 between Balilla and Dular (figs. S1 and S2). Because both ORF5+ and ORF4+ are indispensable for gamete killing, ORF4 is apparently a partner in gamete killing with ORF5.

The results of genetic analysis for the *S5*-induced hybrid sterility presented above are schematically summarized in Fig. 1A. Female gametes in the *indica-japonica* hybrid are killed during sporogenesis by ORF5+ in partner with ORF4+ but protected by ORF3+.

An expression database (*21*) indicated that both *ORF4* and *ORF5* show low expression—almost at the background level throughout the life cycle (fig. S4). *ORF3* transcripts were more abundant, especially in developing panicles. Transient expression assays with rice protoplasts revealed that both ORF3+ and ORF3– proteins localized to the endoplasmic reticulum (ER) (fig. S5, A to H). ORF4+ localized to the plasma membrane and Golgi (fig. S5, Q to T), whereas ORF4– localized to the ER (fig. S5, I to P). ORF5 protein was found in the extracellular domain (*11*).

Microarray analysis of ovaries at the functional megaspore stage showed that *ORF3* expression was statistically significantly higher in Balilla*ORF5*+ transgene-positive than in -negative plants (table S1). We detected an ER stress-responsive UPRE-like *cis*-element (TGACGAGG) (*22*) in the promoter of *ORF3* at –256 bp (fig. S1). Expression of a number of ER stress-responsive genes was also statistically significantly higher in Balilla*ORF5*+ plants (table S1 and fig. S6A). This pattern of induction is highly similar to that observed in ER stress studies in rice (*23*–*25*). As a response to stress (*25*), the ER stress sensor IRE1 transduces signals through the unconventional splicing of *OsbZIP50* mRNA, which causes a frameshift producing a nuclear localization signal in the protein designated OsbZIP50-S, which regulates the expression of many ER stress-responsive genes, including *ORF3*. We confirmed that the spliced *OsbZIP50-S* mRNA was present in Balilla*ORF5*+ plants (fig. S7). Taken together, these results suggested that introduction of *ORF5*+ into Balilla induced ER-stress in ovaries.

Bax inhibitor-1 (BI1) is a conserved ER-resident cell death suppressor in eukaryotes and plays an important role in modulating the ER stress-mediated programmed cell death (PCD) pathway both in *Arabidopsis* and rice (*26*, *27*). Our analysis (fig. S6B) showed that *OsBI1* was up-regulated in Balilla*ORF5*+ plants. *OsKOD1* [an orthologous gene of kiss of death (KOD), which acts as a PCD-inducer in *Arabidopsis*] (*28*) and *Hsr203j* (the commonly used cell death marker) (*24*, *29*) were also up-regulated by *ORF5*+. Expression of *OsCP1*, which acts as an executor of the PCD process in rice tapetum development (*30*, *31*), was elevated by ~12-fold in ovaries of Balilla*ORF5*+ plants. In addition, many differentially expressed genes between Balilla*ORF5*+ transgene-positive and -negative plants revealed in the microarrays (table S2) were PCD-related, such as the cytochrome *P450*, *LTPL*, and *GDSL*

Table 1. Segregation distortion at the *S5* locus detected in F_2 seedlings from various crosses.

Population (or cross)	Generation	*S5* genotype	Number of plants*	χ^2 (1:2:1)	Spikelet fertility (%)†
BL(BL/NJ)‡	BC_6F_2	BL/BL	9 (48.75)	59.5 (P = 0.00)	85.6 ± 2.5 (P = 0.00)§
		BL/NJ	101 (97.5)		52.6 ± 0.6
		NJ/NJ	85 (48.75)		89.5 ± 0.9
Nanjing 11 /Balilla	F_2	BL/BL	10 (46)	106.6 (P = 0.00)	
		BL/NJ	70 (92)		
		NJ/NJ	104 (46)		
Nanjing 11 /Nipponbare	F_2	NP/NP	11 (49.75)	80.1 (P = 0.00)	
		NP/NJ	89 (99.5)		
		NJ/NJ	99 (49.75)		
93-11 /Nipponbare	F_2	NP/NP	18 (53.5)	65.1 (P = 0.00)	
		93/NP	96 (107)		
		93/93	100 (53.5)		

*Numbers in parentheses are expectations based on 1:2:1 ratio for each cross. †Mean ± SEM. ‡Near isogenic line heterozygous for the *S5* fragment developed by crossing Balilla with Nanjing 11 and backcrossed six times with Balilla. BL, Balilla; NP, Nipponbare; NJ, Nanjing 11; 93, 93-11. §*P* value from a *t* test of the heterozygote against the two homozygotes.

Table 2. The effects of *ORF3* and *ORF5* on spikelet fertility.

Line or cross*	Generation	*S5* genotype†	Number of plants	Spikelet fertility (%)‡	*P* value§
Balilla*ORF3*+	T_1	BL/BL	27	85.6 ± 1.2	0.37
		BL/BL*ORF3*+	30	87.1 ± 0.8	
BL(NJ/NJ) × Balilla*ORF3*+	F_1	BL/NJ	23	50.3 ± 0.6	0.00
		BL/NJ*ORF3*+	53	71.5 ± 0.6	
BL(BL/NJ)*ORF3*+	F_2	BL/BL	4	91.0 ± 3.4	
		BL/NJ	5	46.8 ± 0.4	0.00
		NJ/NJ	6	87.5 ± 0.7	
		BL/BL*ORF3*+	10	92.7 ± 1.5	
		BL/NJ*ORF3*+	19	75.1 ± 1.7	
		NJ/NJ*ORF3*+	15	86.6 ± 1.6	
Balilla*ORF3*+ × Balilla*ORF5*+	F_1	BL/BL	3	80.8 ± 0.7	
		BL/BL*ORF3*+	5	82.7 ± 4.4	
		BL/BL*ORF5*+	7	3.9 ± 0.8	0.00
		BL/BL*ORF3*+*ORF5*+	13	47.7 ± 2.7	

*BL(NJ/NJ) and BL(BL/NJ) indicate near-isogenic lines in Balilla background with the *S5* locus homozygous for the fragment from NJ (Nanjing 11), or heterozygous for NJ and BL (Balilla) fragments. †BL, Balilla; NJ, Nanjing 11. ‡Mean ± SEM. §*P* value obtained by *t* test between the two genotypes in the same cross or selected genotypes in the same shade.

gene families (*31*). These results suggested that ORF5+-induced ER stress might provoke abnormal PCD in embryo-sac development. We performed a terminal deoxynucleotidyl transferase-mediated deoxy-uridine 5′-triphosphate (dUTP) nick-end labeling (TUNEL) assay for PCD by detecting DNA fragmentation during female sporogenesis (fig. S8). No cellular abnormality or TUNEL signal was observed before meiosis (fig. S8, A and B). Cellular abnormality was observed in megasporocyte undergoing meiosis and afterward in Balilla*ORF5+* (fig. S8, C to J). TUNEL signal occurred earlier and stronger in Balilla*ORF5+* than in Balilla (fig. S8, C to J). Thus, premature PCD occurred during female sporogenesis in Balilla*ORF5+*, resulting in embryo-sac abortion. In contrast, introduction of *ORF3+* into Balilla*ORF5+* plant by crossing Balilla*ORF5+* with homozygous Balilla*ORF3+* restored normal expression levels of the ER stress-responsive and PCD-related genes in the hybrid (fig. S9). This implies that ORF3+ is a suppressor of ORF5+-induced ER stress and subsequent PCD.

On the basis of these results, we hypothesize (Fig. 1B) that the activity of extracellular ORF5+ produces a molecule that is sensed by plasma membrane–localized ORF4+ and eventually triggers ER stress. The ER stress subsequently actuates the IRE1-mediated splicing of *OsbZIP50* mRNA, producing OsbZIP50-S, a transcription factor that turns on expression of ER stress-responsive genes, including *ORF3*. The ER stress is resolved in the presence of ORF3+, thus producing normal female gametes. Whereas in the absence of ORF3+, unresolved ER stress induces PCD-related genes, causing anomalous PCD, which leads to embryo-sac abortion, despite the presence of OsBI1. Thus, proteins encoded by *ORF3*, *ORF4*, and *ORF5* are elements involved in different stages of the ER stress-induced PCD pathway regulating hybrid fertility.

We obtained sequences of *ORF3*, *ORF4*, and *ORF5* for 82 accessions of *O. sativa*, *O. rufipogon*, and *O. nivara* from 16 countries over a diverse geographical area (table S3). Nineteen haplotypes were identified containing single-nucleotide polymorphisms (SNPs) and insertions/deletions (Indels) in the coding sequence of *ORF3* (fig. S10). Four of the haplotypes could be placed in the *ORF3–* allele group, and 15 classified into the *ORF3+* allele group. Five of the 18 haplotypes detected for *ORF4* were classified into the *ORF4–* group and 13 into the *ORF4+* group. Together with the three allelic groups identified in *ORF5* (*ORF5+*, *ORF5–*, and *ORF5n*) (*32*), there are a total of 12 possible combinations formed of the three genes. We observed 9 of the 12 combinations (table S4). *ORF3+*, *ORF4+*, and *ORF5+* was the most common, especially in the two wild rice species *O. rufipogon* and *O. nivara*. This represents a balance between killing and protecting the gametes, according to our genetic model. The sequence of the outgroup *O. glumaepatula* suggested that *ORF3+*, *ORF4+*, and *ORF5+* is the ancestral type. The suicidal combination of *ORF3–*, *ORF4+*, and *ORF5+*, which would not be able to survive in nature, was not observed in the sample, although it would be the easiest to be generated at the population level through mutation and/or recombination. Two other combinations (*ORF3–*, *ORF4–*, and *ORF5+* and *ORF3–*, *ORF4–*, and *ORF5–*) were not detected because of either their rarity or the source of sample. This result was congruent to the proposed genetic model of the killing-protecting system. The typical *indica*-like (*ORF3+*, *ORF4–*, and *ORF5+*) and *japonica*-like (*ORF3–*, *ORF4+*, and *ORF5–*) types were found in wild rice accessions, suggesting that the ancestors of *indica* and *japonica* rice probably originated before domestication. Because *indica* and *japonica* rice (also *indica-like* and *japonica-like* wild rice) have distinct ranges of distribution worldwide, geographical isolation might have played an important role in maintaining distinctions of the rice groups as well as the killer-protector system. This killer-protector system may have a profound implication in the evolution and diversification of rice. Reproductive isolation enforced by the killer (ORF4+, ORF5+) would have promoted genetic differentiation between *indica* and *japonica* rice, which appears to be a major source of genetic diversity in the rice gene pool, whereas the protector (ORF3+) and nonkiller combinations of ORF4 and ORF5 would allow for hybridization and gene flow, thus providing a coherent force at the species level.

Table 3. The effects of *ORF4* and *ORF5* on spikelet fertility and segregation distortion.

Line or cross	Generation	*S5* genotype	Number of plants	Spikelet fertility (%)*	*P* value
BL(NJ/NJ)*ORF4+*	T_1	NJ/NJ	24	87.0 ± 0.7	0.31†
		NJ/NJ*ORF4+*	26	89.3 ± 1.3	
BL(BL/DL) × BL(BL/NJ)	F_1	BL/BL	19	84.7 ± 0.9	0.00‡
		BL/DL	16	86.0 ± 1.1	
		BL/NJ	20	51.4 ± 1.0	
		DL/NJ	23	81.8 ± 1.5	
BL(NJ/NJ)*ORF4+* × BL(DL/DL)	F_1	DL/NJ	22	79.1 ± 2.6	0.00†
		DL/NJ*ORF4+*	28	39.3 ± 1.9	
BL(DL/NJ)*ORF4+*	F_2	DL/DL	5 (19.5)§		0.00§
		DL/NJ	44 (39)		
		NJ/NJ	29 (19.5)		
Balilla*ORF5+*	T_2	BL/BL	8	86.9 ± 1.7	
		BL/BL*ORF5+*	22	0.01 ± 0.3	
BL(BL/DL) × Balilla*ORF5+*	F_1	BL/BL	10	90.7 ± 1.2	
		BL/DL	10	88.8 ± 0.6	0.00‖
		BL/BL*ORF5+*	12	1.0 ± 0.2	
		BL/DL*ORF5+*	24	5.9 ± 0.9	
BL(BL/DL)*ORF5+* from: BL(BL/DL) ×Balilla*ORF5+*	F_2	BL/BL	4	91.8 ± 3.7	
		BL/DL	7	90.9 ± 1.8	0.00‖
		DL/DL	2	90.9 ± 1.8	
		BL/BL*ORF5+*	16	0.7 ± 0.3	
		BL/DL*ORF5+*	16	3.0 ± 1.1	
		DL/DL*ORF5+*	9	90.6 ± 1.3	
BL(NJ/NJ) × Balilla*ORF5+*	F_1	BL/NJ	14	52.6 ± 0.4	0.51†
		BL/NJ*ORF5+*	17	52.2 ± 0.5	

*Mean ± SEM. †Probability obtained from a *t* test between the two genotypes of the same cross. ‡Probability obtained from a *t* test of BL/NJ genotype against the other three genotypes in the same cross. §Probability obtained from a χ^2 test; expected numbers based on 1:2:1 ratio are in parentheses. ‖Probability obtained from a *t* test between the shaded genotypes in the same cross. BL, Balilla; DL, Dular; NJ, Nanjing 11.

References and Notes

1. J. A. Coyne, H. A. Orr, *Speciation* (Sinauer Associates, Sunderland, MA, 2004).
2. T. W. Lyttle, *Annu. Rev. Genet.* **25**, 511 (1991).
3. A. Burt, R. Trivers, *Genes in Conflict: The Biology of Selfish Genetic Elements* (Belknap Press, Cambridge, MA, 2006).
4. K. Bomblies, D. Weigel, *Nat. Rev. Genet.* **8**, 382 (2007).
5. D. Bikard *et al.*, *Science* **323**, 623 (2009).
6. R. Alcázar, A. V. García, J. E. Parker, M. Reymond, *Proc. Natl. Acad. Sci. U.S.A.* **106**, 334 (2009).
7. K. Bomblies, *Annu. Rev. Plant Biol.* **61**, 109 (2010).
8. K. Liu, Z. Zhou, C. Xu, Q. Zhang, M. A. Saghai Maroof, *Euphytica* **90**, 275 (1996).
9. Y. Ouyang, Y. G. Liu, Q. Zhang, *Curr. Opin. Plant Biol.* **13**, 186 (2010).
10. Y. Ouyang, J. Chen, J. Ding, Q. Zhang, *Chin. Sci. Bull.* **54**, 2332 (2009).
11. J. Chen *et al.*, *Proc. Natl. Acad. Sci. U.S.A.* **105**, 11436 (2008).
12. Y. Long *et al.*, *Proc. Natl. Acad. Sci. U.S.A.* **105**, 18871 (2008).
13. Y. Mizuta, Y. Harushima, N. Kurata, *Proc. Natl. Acad. Sci. U.S.A.* **107**, 20417 (2010).
14. Y. Yamagata *et al.*, *Proc. Natl. Acad. Sci. U.S.A.* **107**, 1494 (2010).
15. H. Ikehashi, H. Araki, in *Rice Genetics*, International Rice Research Institute (IRRI), Eds. (IRRI, Manila, Philippines, 1986), pp. 119–130.
16. S. Yanagihara *et al.*, *Theor. Appl. Genet.* **90**, 182 (1995).
17. K. Liu *et al.*, *Theor. Appl. Genet.* **95**, 809 (1997).
18. S. Q. Qiu *et al.*, *Theor. Appl. Genet.* **111**, 1080 (2005).
19. C. Wang, C. Zhu, H. Zhai, J. Wan, *Genet. Res.* **86**, 97 (2005).

20. Y. Koide *et al.*, *Genetics* **180**, 409 (2008).
21. L. Wang *et al.*, *Plant J.* **61**, 752 (2010).
22. H. Yoshida *et al.*, *Dev. Cell* **4**, 265 (2003).
23. Y. Oono *et al.*, *Plant Biotechnol. J.* **8**, 691 (2010).
24. Y. Wakasa *et al.*, *Plant J.* **65**, 675 (2011).
25. S. Hayashi, Y. Wakasa, H. Takahashi, T. Kawakatsu, F. Takaiwa, *Plant J.* **69**, 946 (2012).
26. N. Watanabe, E. Lam, *J. Biol. Chem.* **283**, 3200 (2008).
27. H. Matsumura *et al.*, *Plant J.* **33**, 425 (2003).
28. R. Blanvillain *et al.*, *EMBO J.* **30**, 1173 (2011).
29. D. Pontier, M. Tronchet, P. Rogowsky, E. Lam, D. Roby, *Mol. Plant Microbe Interact.* **11**, 544 (1998).
30. S. Lee, K.-H. Jung, G. An, Y.-Y. Chung, *Plant Mol. Biol.* **54**, 755 (2004).
31. H. Li *et al.*, *Plant Physiol.* **156**, 615 (2011).
32. H. Du, Y. Ouyang, C. Zhang, Q. Zhang, *New Phytol.* **191**, 275 (2011).

Acknowledgments: We thank D. S. Brar of the International Rice Research Institute for providing the rice seeds, and S. Luan of University of California, Berkeley, USA for discussion. This research was supported by grants from the National Natural Science Foundation (31130032 and 30921091), the 863 Project (2012AA100103), and the 111 Project (B07041) of China. All of the DNA sequences obtained in this study have been deposited in the GenBank from accession codes JX138498 to JX138505. A patent for the ORF5 sequence has been approved by the State Intellectual Property Office of China (ZL200710053552.9).

Supplementary Materials

www.sciencemag.org/cgi/content/full/337/6100/1336/DC1
Materials and Methods
Figs. S1 to S10
Tables S1 to S7
References (*33*–*41*)

23 April 2012; accepted 13 June 2012
10.1126/science.1223702

Single Reconstituted Neuronal SNARE Complexes Zipper in Three Distinct Stages

Ying Gao, Sylvain Zorman, Gregory Gundersen, Zhiqun Xi, Lu Ma, George Sirinakis, James E. Rothman,* Yongli Zhang*

Soluble *N*-ethylmaleimide–sensitive factor attachment protein receptor (SNARE) proteins drive membrane fusion by assembling into a four-helix bundle in a zippering process. Here, we used optical tweezers to observe in a cell-free reconstitution experiment in real time a long-sought SNARE assembly intermediate in which only the membrane-distal amino-terminal half of the bundle is assembled. Our findings support the zippering hypothesis, but suggest that zippering proceeds through three sequential binary switches, not continuously, in the amino- and carboxyl-terminal halves of the bundle and the linker domain. The half-zippered intermediate was stabilized by externally applied force that mimicked the repulsion between apposed membranes being forced to fuse. This intermediate then rapidly and forcefully zippered, delivering free energy of 36 k_BT (where k_B is Boltzmann's constant and T is temperature) to mediate fusion.

Soluble *N*-ethylmaleimide–sensitive factor attachment protein receptor (SNARE) proteins mediate membrane fusion in the cell, and in particular the fusion of vesicles stored at nerve endings to release neurotransmitters for synaptic transmission (*1*, *2*). The neuronal SNAREs consist of vesicle-associated membrane protein 2 (VAMP2, also called synaptobrevin) on the vesicle membrane (v-SNARE) and the binary complex of syntaxin 1 and SNAP-25 on the plasma membrane (target or t-SNARE) (*3*, *4*). Together these SNAREs drive membrane fusion by joining into a parallel four-helix bundle (*4*), which is envisioned to zipper progressively toward the membranes (*5*), providing force that overcomes an estimated energy barrier of >40 k_BT (where k_B is Boltzmann's constant and T is temperature) (*6*). Considerable indirect evidence favors the zippering hypothesis (*7*–*12*), but direct observation of the assembly intermediates and accurate characterization of the zippering energy and kinetics have been lacking.

We developed a single-molecule manipulation assay to investigate SNARE assembly based on high-resolution dual-trap optical tweezers (Fig. 1A). We cross-linked the N termini of syntaxin and VAMP2 by a disulfide bridge and attached syntaxin by its C terminus to one bead and VAMP2 to another through a DNA handle (*13*). The experiment was started with a single preassembled SNARE complex containing truncated syntaxin (187–265) and VAMP2 (25–92) and full-length SNAP-25 (*4*, *14*) to avoid misassembled SNARE by-products (*10*, *15*).

The protein-DNA conjugate extended with the increasing pulling force in a nonlinear manner predicated by the worm-like chain model (Fig. 1B and fig. S2). However, the monotonic force and extension curves were interrupted by abrupt changes caused by SNARE disassembly or reassembly (Fig. 1C). Fast reversible transitions appeared in two force regions, the first in the range of 8 to 13 pN with ~3-nm average extension change (Fig. 1D and fig. S3) and the second in the range of 14 to 19 pN with ~7-nm extension change (Fig. 1D and fig. S4). Both transitions occurred between two states (fig. S5 and table S1), manifesting two distinct binary switches in SNAREs. When the linker domain (LD) of VAMP2 was deleted, the first transition disappeared, whereas the second transition remained (fig. S6). Thus, the first transition is caused by reversible folding and unfolding of the LD alone. The average size of the extension change suggests that a total of 22 (±3, SD) amino acids or 10 amino acids in VAMP2 (83–92) participated in the transition (fig. S7A). This observation is consistent with a fully zippered LD in a coiled-coil conformation in solution (Fig. 1B, state 1) as seen in the crystal structure of the SNARE complex (*4*, *16*). Further deletion into the C-terminal SNARE domain of VAMP2 (Vc) abolished the second transition (fig. S8), which suggests that this VAMP2 region is involved in the transition.

The additional ~7-nm extension increase from the LD unfolded state (Fig. 1B, state 2) leads to a partially zippered SNARE state (state 3, Fig. 1E). To derive the structure, energy, and kinetics associated with this state, we measured the real-time transition involving Vc at different mean forces (Fig. 1D). The fast two-state transition was confirmed by hidden-Markov modeling (HMM) (*17*) and the histogram distribution of extension (figs. S5B and S9). On the basis of the measured extension change and an asymmetrical transition model (fig. S10) (*18*), we found that 26 (±3) amino acids in VAMP2 (57–82) were unzipped in the partial SNARE complex (Fig. 1E). This places the interface of the unzipped Vc and the zippered N-terminal VAMP2 (Vn) at residue 56 (±5, SD; ±1, SEM) or at the central ionic layer of the bundle. This ionic layer is one of the most evolutionarily conserved features of all SNAREs (*19*), yet with unclear functions. Thus, our result suggests a possible role of the ionic layer in stabilizing the half-zippered neuronal SNARE structure crucial for regulation of membrane fusion (*7*, *8*, *12*, *18*, *20*).

The half unfolding probability of Vc (Fig. 2A) determines an average equilibrium force (f_{eq}) of 17 (±2 SD, n = 76) pN, which can be defined as the maximum force output of Vc zippering averaged over the accompanying extension change. This force is the highest equilibrium force reported for any coiled-coil proteins (*17*), including the designed strongest known coiled coil designated as pIL with an equilibrium force of 12.4 pN (*21*). The unfolding probability could be extrapolated to zero force (*14*, *17*, *22*) to reveal the Vc zippering free energy of 28 (±3) k_BT, higher than the folding energy of pIL [24 (±1) k_BT] despite pIL's greater length (33 amino acids) (*21*).

The average Vc zippering rate at the maximum force output (~160 s^{-1}) (Fig. 2B) is also greater than the equilibrium rate of pIL (~10 s^{-1}) (*21*). Yet the rate is much less than the estimated

Department of Cell Biology, Yale University School of Medicine, 333 Cedar Street, New Haven, CT 06520, USA.

*To whom correspondence should be addressed. E-mail: yongli.zhang@yale.edu (Y.Z.); james.rothman@yale.edu (J.E.R.)